Doi: https://doi.org/10.63333/eem.v2n11 Vol. 2 No. 1 (2026)

The Al_2O_3 particle reinforced Al-Fe composites fabricated through an in-situ reaction of Fe_2O_3 powders in Al melts

Hao Lian, Wenlong Yu, Z. M. Shi*

School of Materials Science and Engineering, Inner Mongolia University of Technology, Hohhot, 010051, China; Tel/Fax: 86-471-6575752
* Correspondence: shizm@imut.edu.cn

Abstract: Al-Fe alloys possess excellent ability to resist heat and wear. However, their mechanical properties are greatly deteriorated due to the coarse needle-like and plate-like Al_3Fe phases segregating the soft Al matrix. In this study, the Al_2O_3 particle-reinforced Al-1.8 wt% Fe and Al-5.0 wt% Fe composites were prepared via an in-situ reaction of Fe_2O_3 powders in Al melts, the effects of Al_2O_3 particles on microstructure and mechanical properties were systematically investigated. Results show that the composites can be prepared through a reduction reaction of Fe_2O_3 powders in stirring Al melts at 1200 ℃ for 30 min. The densely dispersed Al_2O_3 particles refine the microstructure by inhibiting growths of α-Al grains and Al_3Fe phases. The mechanical properties of composites are improved by grain refinement and secondary-phase strengthening. The yield strength, tensile strength, elongation, and hardness are increased by 32.3%, 52.7%, 57.1%, and 28.8% for Al-1.8 Fe composite and 18.0%, 51.1%, 150.0%, and 21.1% for Al-5 Fe composite respectively when compared with their corresponding alloys. These composites, combined with high strength, plasticity, and hardness, are promising materials for applications in energy and environment fields.

Keywords: Al-Fe; composite; in-situ reaction; Al_2O_3 particles; microstructure; mechanical property

1. Introduction

Al-Fe alloys are lightweight structural materials with excellent resistance to wear and heat due to the chemically-thermally stable Al_3Fe intermetallics existing in the Al matrix [1]. These materials are widely employed to fabricate key components, including radiators, electric cables, cable cladding, and equipment housings in the fields of energy and environmental engineering, where service conditions often involve high temperatures, particle erosion, and chemical corrosion. However, when the Fe content exceeds 0.11 wt%, the coarse needle-like and flake-like Al_3Fe phases are formed in the alloys, especially in hypereutectic alloys, where the plate-like, flower-like, and bulky Al_3Fe phases are produced. These phases act as initiation sites of microcracks during plastic deformation and service, significantly worsening the mechanical properties and plastic workability of alloys [2–3]. Extensive researches are conducted to mitigate the detrimental effects of coarse Fe-rich phases.

To refine the microstructure through melt modification, Song et al. [4] regulated the morphology of coarse Fe-rich phases by adding 0.4 wt% Cr elements; the Cr adsorbs on the surface of Al_3Fe phases to inhibit their orientation growth and so refine the microstructure; however, excessive addition (>0.8 wt%) leads to occurrence of the coarse Al–Fe–Cr ternary phases again. Vončina et al. [5] prepared a rare earth (Ce/La) modified Al–1.4 Fe alloy; the rare earth elements enrich at the solidification front of primary α-

Doi: https://doi.org/10.63333/eem.v2n11 Vol. 2 No. 1 (2026)

Al grains and eutectic Al_3Fe phases to inhibit their preferential growth to refine the phases. Qin et al. [6] investigated the effect of Ni on the microstructure and properties of Al–1Fe alloy; Ni addition effectively refines α-Al grains and forms Al_9FeNi phases, improving the strength but reducing ductility and electrical conductivity. The optimized Ni addition of 6.0 wt% leads to a remarkable increase in tensile strength due to the grain refinement and second-phase strengthening effect.

Utilization of advanced processing techniques is also useful for refinement of the microstructure. Nayak et al. [7] fabricated Al–10 Fe alloys via rapid solidification, which produces a multiphase system of amorphous, nano-quasicrystalline, and Al_5Fe_2 phases. The obtained alloy achieves an ultrahigh tensile strength of 3.57 GPa by the synergistic effects of solid solution strengthening (9.17 at.% Fe solubility in Al matrix), dispersion strengthening of nano-quasicrystalline phases, and fine grain strengthening of nanoscale α-Al grains (20–30 nm). Medvedev et al. [8] combined electromagnetic casting and severe plastic deformation to refine microstructure and enhance properties of Al–0.5 Fe and Al–2.5 Fe alloys. This processing route produces an ultrafine grain structur and high tensile strength of 200.0 MPa and 340.0 MPa, respectively. Chen et al.[9] employed continuous rheo-extrusion and rolling to achieve multi-stage refinement of microstructure and improvement of mechanical properties of a Al–3 Fe alloy. The generated nano-/submicron Al_3Fe phases ensure a strength superior to that of pure Al. The comprehensive mechanical properties were obtained at a rolling deformation of 90% due to grain refinement and formation of high-density substructures.

The in-situ reaction synthesis of particle-reinforced aluminum composites offers a promising alternative to conventional methods for enhancing mechanical performance [10]. Lian et al. [11] synthesized spinel particle-reinforced Al-2Fe composites via an in-situ reaction technology; the uniformly dispersed spinel particles refine the α-Al grains and Al_3Fe phases by 54.7% and 34.5%, respectively. As the particles act as nucleation substrates for α-Al and Al_3Fe crystals, the alloy's mechanical properties are substantially enhanced. Su et al. [12] fabricated a nano-Al_2O_3p/2024 composite using a solid-liquid mixing casting combined with an ultrasonic treatment; the ultrasonic processing refines the α-Al grains and improves the distribution of reinforcements simultaneously, leading to increases of 37% in tensile strength and 81% in yield strength for the composite containing 1.0 wt.% Al_2O_3. Wang et al. [13] produced Al_2O_3 p/Al composites through an in-situ reaction between CeO_2 and Al molts. The in-situ formed particles have a size of 100–200 nm, but no crystallographic orientation relationship stimulates nucleation of α-Al grains. Even this. The fine particles still contribute a synergistic strengthening effect by secondary phase (particle), dislocations, and fine subgrains. Zhu et al. [14] fabricated α-Al_2O_3 particles and Ni_2Al_3 intermetallic co-reinforced composites via an exothermic reaction in Al-Ni_2O_3 system; the reaction is a spontaneous process with a two-step reaction at activation energies of 457.3 kJ/mol and 282.4 kJ/mol, respectively. The Ni_2Al_3 intermetallics is uniformly distributed in the matrix; the α-Al_2O_3 particles show a slight segregation. The strength of composite is mainly governed by the Ni_2Al_3 phases; the highest tensile strength of 210 MPa and elongation of 8% are achieved at a reinforcement volume fraction of 30%.

The liquid-solid in-situ reaction technology is extensively studied for preparation of aluminum based composites, especially used for the large castings in engineering [15-18], however, it was barely applied in the Al-Fe based composites. This study employed the liquid-solid reduction of Fe_2O_3 powders in Al melts to prepare Al_2O_3 particle-reinforced Al-Fe composites. The micro and nano-sized Al_2O_3 particles are directly generated in Al melts through the reduction reaction of Fe_2O_3+Al=Fe+Al_2O_3. It is expected that the Al_2O_3 particles can improve the microstructure and mechanical properties of the alloys by refinement of Al grains and Fe-rich phases and by strengthening and toughening of the Al matrix.

The Al_2O_3 particle reinforced Al-Fe based composites exhibit more advantages than the Al-Fe alloys in terms of preparation, microstructure, and mechanical property. First, the reduced Fe elements can leave out addition of Fe-containing raw material. Second, introduction of the hard Al_2O_3 particles can enhance the wear resistance and high-temperature stability of the alloys [19-21]; these properties are fundamental for the Al-Fe alloys. It must be noted that this in-situ reaction of Fe_2O_3 in Al melts is only suitable for the Al-Fe system, this is because higher amount of Fe elements are not desired in other Al alloys.

Doi: https://doi.org/10.63333/eem.v2n11 Vol. 2 No. 1 (2026)

2. Experimental

Two kinds of Al–Fe composite materials with compositions of 1.8 wt% and 5.0 wt% Fe were prepared using raw materials of industrial-pure aluminum ingot and Fe_2O_3 powder. The usage of Fe_2O_3 powder was stoichiometrically calculated based on the targeted Fe contents. The furnace was heated to 750 °C, the aluminum ingot was added to a graphite crucible and put it in the furnace to completely melt. The melts was stirred at 300 rpm with a graphite rod to form a vortex. The preheated Fe_2O_3 powders (200 °C) sealed with aluminum foil were introduced into the vortex under continuous stirring. The temperature was raised to the preset reaction temperatures of 1000 °C, 1100 °C, and 1200 °C, respectively, at a speed of 20 °C/min, held for 30 min to ensure complete reaction. At this time, the furnace was full of Ar atmosphere to avoid melts oxidizing. Finally, the melts was cooled to 750 °C at a speed of nearly 10 °C/min in the furnace, stirred for 5 min at a speed of 150 rpm, stood for 5 min, and poured into a preheated steel mold (250 °C, wall thickness of 15 mm, cavity thickness of 18 mm) to obtain ingots. The ingot samples were machined into specimens (ϕ15 × 30 mm) for subsequent analysis and testing. Table 1 shows the chemical composition of both samples.

Table 1. The main chemical composition of samples, wt%

Composites	Fe	Si	Al
Al-1.8 Fe	1.76	0.06	Bal.
Al-5 Fe	5.20	0.07	

The thermal reaction behavior of Al-Fe_2O_3 system was studied using differential scanning calorimetry (TA Instruments SDT 650) under an argon atmosphere, with a heating rate of 10 °C/min. The phase composition was analyzed using an X-ray diffraction (D/MAX-2500/PC) with CuKα target, at a voltage of 40 V, current of 100 mA, and a scanning rate of 3/min. The microstructure was examined by a scanning electron microscopy (FEI Quanta 650). Quantitative analysis of the size and quantity of Fe-rich phases was performed using an Image-Pro Plus 6.0 software. The mechanical properties of samples were tested using a universal testing machine (5982, Instron) at a loading speed of 1.5 mm/min. The hardness was inspected by a Vickers hardness tester (FM-810, Future-Tech) using a diamond pyramid indenter with a diameter of 5.0 mm and a pressure of 250 g for 15 s. Five samples were used for each group to obtain the averages of properties.

3. Results and discussion

3.1 Thermodynamic analysis of potential reactions

Table 2 shows the Gibbs free energy as a function of temperature for potential reactions in Al-Fe_2O_3 system.

Gibbs free energy (ΔG_T^Θ) was calculated using following equations:

$$\Delta G_T^\Theta = \Delta H_T^\Theta - T\Delta S_T^\Theta \quad (1)$$

$$\Delta H_T^\Theta = \Delta H_{298}^\Theta + \int_{298}^{T} \Delta C_P dT \quad (2)$$

$$\Delta S_T^\Theta = \Delta S_{298}^\Theta + \int_{298}^{T} \frac{\Delta C_p}{T} dT \quad (3)$$

Where, ΔH_{298}^Θ is the enthalpy change of the system at the standard temperature; $\Delta S_{298}^\Theta$is the entropy change of the system at the standard temperature; $\Delta H_T^\Theta$is the enthalpy change of the system; $\Delta S_T^\Theta$is the entropy change of the system; $\Delta C_P$is the heat capacity difference ($\Delta C_p = a + b\times10^{-3}T - c\times10^{5}T^{-2}$); $\Delta G_T^\Theta$is the Gibbs free energy of the reaction. These thermodynamic constants are derived from the Handbook of Practical Inorganic Thermodynamic Data [22].

All the reactions exhibit negative Gibbs free energy in the practical melting temperature, indicating that they are thermodynamically spontaneous. Under conditions of Al-rich and enough soaking time, all

Doi: https://doi.org/10.63333/eem.v2n11 Vol. 2 No. 1 (2026)

of the intermediate phases of Fe_3O_4, FeO, $FeAl_2O_4$ can be finally transformed into the stablest Al_2O_3 and Al_3Fe phases.

Table 2. The potential reactions and relationships between Gibbs free energy and temperature.

Reactions	Gibbs Free Energy (kJ/mol)	ΔG_T^Θ at given temperatures (KJ/mol)
$2Al_{(L)}+Fe_2O_{3(S)}=2[Fe]+Al_2O_{3(S)}$	$\Delta G_1^\Theta=-853.8+0.04T$	-805.8, 1200 °C
$2Al_{(L)}+3Fe_2O_{3(S)}=2Fe_3O_{4(S)}+Al_2O_{3(S)}$	$\Delta G_2^\Theta=-465.2+0.1T$	-345.2, 1200 °C
$2Al_{(L)}+Fe_3O_{4(S)}=3FeO_{(S)}+Al_2O_{3(S)}$	$\Delta G_3^\Theta=-324.5+0.06T$	-252.5, 1200 °C
$8Al_{(L)}+3Fe_3O_4=9[Fe]+4Al_2O_{3(S)}$	$\Delta G_4^\Theta=-2845.6+0.3T$	-2485.6, 1200 °C
$FeO_{(S)}+Al_2O_{3(S)}=FeAl_2O_{4(S)}$	$\Delta G_5^\Theta=-38.9+0.01T$	-26.9, 1200 °C
$2Al_{(L)}+3FeAl_2O_{4(S)}=3[Fe]+4Al_2O_{3(S)}$	$\Delta G_6^\Theta=-725.4+0.09T$	-617.4, 1200 °C
$3Al_{(L)}+[Fe]=Al_3Fe_{(S)}$	$\Delta G_7^\Theta=-76.1+0.01T$	-69.1, 700 °C
$Al_{(L)}+[Fe]=AlFe_{(S)}$	$\Delta G_8^\Theta=-52.3+0.01T$	-45.3, 700 °C

3.2 DSC curve analysis

The reaction process of Al-Fe_2O_3 system was analyzed using Al and Fe_2O_3 mixed powders as raw materials (Fig. 1). The DSC curve reveals an endothermic peak at 662 °C, which is ascribed to the melting of Al powders. Starting from 955°C, a series of undulating small exothermic peaks appear, which correspond to the incubation of the Al-Fe_2O_3 reaction. As the temperature increased, a pronounced exothermic peak was observed in the range of 1125–1147°C, which marks the main reaction of Al-Fe_2O_3 system. Therefore, the reaction temperature was determined to be 1200 °C to ensure complete reaction and minimizing of oxidation of Al molten.

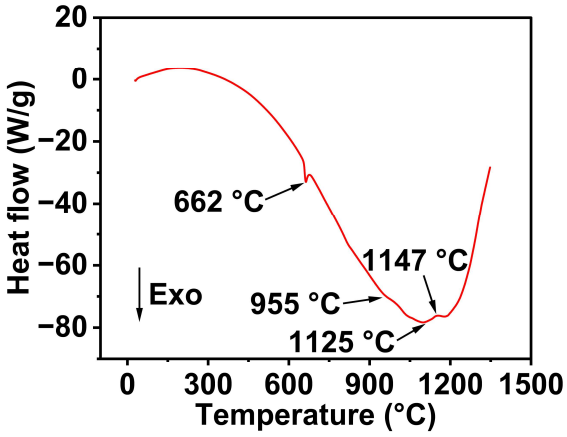

Fig. 1 DSC curve of Al-Fe_2O_3 mixed powders.

3.3 Effect of reaction temperature on the microstructure of composites

To examine the real reaction process, the reaction temperatures were set at 1000 °C, 1100 °C, and 1200 °C respectively.

3.3.1 Al-1.8 Fe composites

The microstructure and IPP results of Al-1.8 Fe composites at three temperatures are shown in Fig. 2. It was observed that the reaction is ignited at 1000 °C because the Fe-rich phases exist in the form of

Doi: https://doi.org/10.63333/eem.v2n11 Vol. 2 No. 1 (2026)

needles at the Al grain boundaries (Fig. 2a). However, the size of Al grains is significantly coarse and nonuniform, the reaction is not completed, and many pores occur in the matrix. When the temperature raised to 1100 °C (Fig. 2b), the size of α-Al grains is greatly decreased and gets more uniform, the Fe-rich phases are distributed at grain boundaries and the pore defects are reduced. When the reaction temperature reaches to 1200 °C (Fig. 2c), the size of α-Al grains is largely reduced, and the Fe-rich phases are mostly small particles with a significant reduction in porosity.

Fact that the reaction occurs at 1000 °C, below the initial temperature of 1125 °C, is ascribed to a local reaction at the contacting interface. This is because the Al atoms in melts adsorb on the surface of Fe_2O_3 particles, which forms a contact interface at an atomic level to easily ignite the reaction; the reaction heat is relatively low and dispersed into melts by stirring. This makes the detector not sense the weaker change in temperature of melts. However, this reaction is slow; preparation at this temperature is not accepted.

Table 3 presents the quantitative statistical results of Fe-rich phases. As the temperature increases from 1000 °C, 1100 °C to 1200 °C, the average diameter of Fe-rich phases decreases from 7.98 μm, 6.82 μm to 5.67 μm, the total number increases from 188, 289 to 1116. This indicates a significant refinement of the Fe-rich phases at 1200°C.

The Fe-rich phases in the composite are supplied by the reduced Fe elements. The reaction also leads to a gradual increase in Al_2O_3 particles, which effectively inhibit the growth of α-Al grains and Fe-rich phases. Moreover, the ultra-high reaction temperature completely removes possible heterogeneous nucleation sites to greatly increase the supercooling trend for crystallization, achieving a refining effect of the microstructure. Thus, the Al-1.8Fe composite with the finest microstructure was obtained at the reaction temperature of 1200 °C.

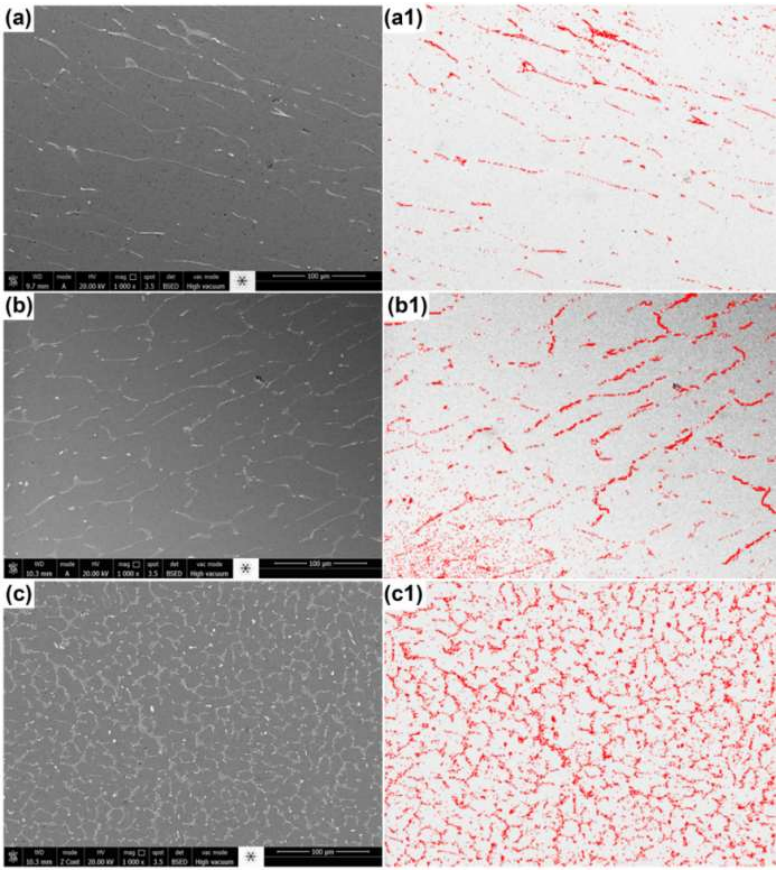

Fig.2 SEM morphology and IPP result of Al-1.8 Fe composites at different reaction temperatures. (a) 1000 °C; (b) 1100 °C; (c) 1200 °C.

Doi: https://doi.org/10.63333/eem.v2n11 Vol. 2 No. 1 (2026)

Table 3 The IPP analytic results of Fe-rich phases

Reaction temperature (°C)	1000	1100	1200
Average diameter (μm)	7.98	6.82	5.67
Average area (μm$_2$)	35.16	26.52	19.17
Total number	188	289	1116

3.3.2 Al-5Fe composite

Fig. 3 shows the microstructure and IPP results of the Al-5 Fe composite. The coarse flower-like Fe-rich phases were observed at 1000 °C (Fig. 3a). Numerous pores occur; this is because the higher powder content increases the melt's viscosity to hinder the gas expulsion. At 1100 °C (Fig. 3b), the granular and short rod-like Fe-rich phases uniformly distribute with reduced size and fewer pore defects. When the temperature reaches to 1200 °C (Fig. 3c), the Fe-rich phases achieve the maximum homogeneity and are further refined into spherical and flake-like shapes, and virtually all pore defects are eliminated.

Table 4 presents the quantitative statistical results of Fe-rich phases in Al-5 Fe composites obtained at three temperatures. As the reaction temperature increases, the average area and average size of Fe-rich phases are decreased, the total number is increased. These parameters show minimal changes between the preparation temperatures of 1000 °C and 1100 °C. However, when the temperature reaches to 1200 °C, the average size and area are remarkably decreased. This indicates that the strongest refinement effect on iron-rich phases is achieved at the reaction temperature of 1200 °C.

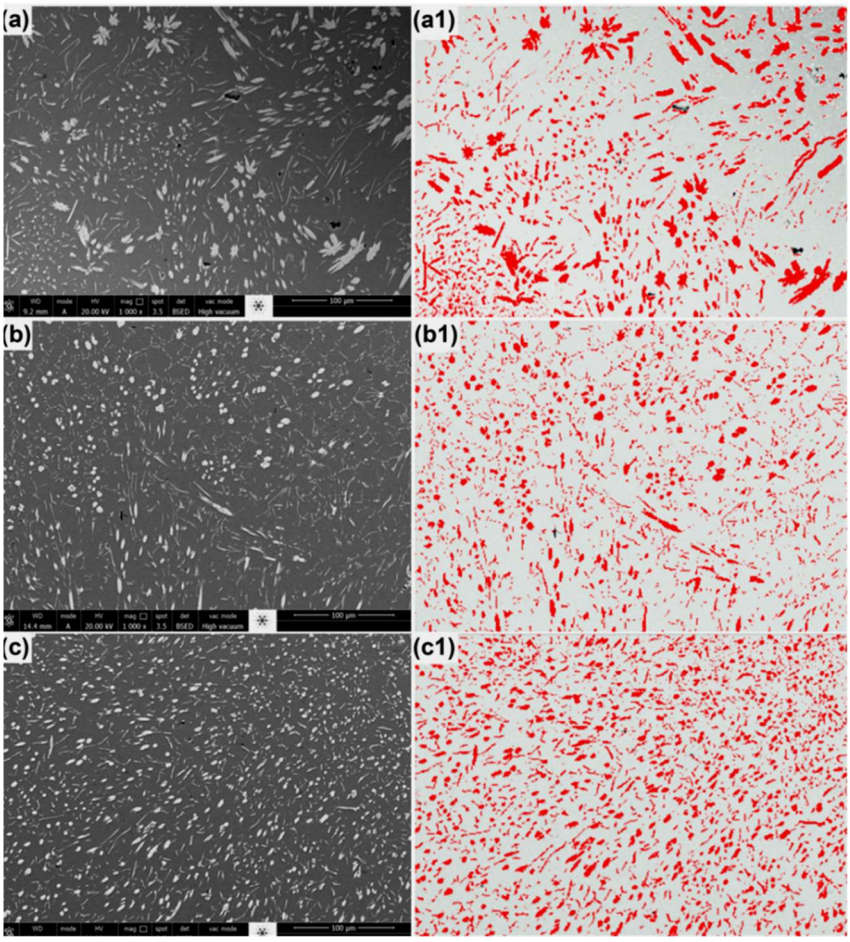

Fig. 3 SEM morphology and IPP analytic result of Al-5Fe composites at different reaction temperatures. (a) 1000 °C; (b) 1100 °C; (c) 1200 °C.

Doi: https://doi.org/10.63333/eem.v2n11 Vol. 2 No. 1 (2026)

Table 4 The IPP analytic result of Fe-rich phases

Reaction temperature (°C)	1000	1100	1200
Average diameter (μm)	13.59	11.87	10.52
Average area (μm_2)	112.91	101.30	86.44
Total number	1008	1014	2004

Fig. 4 shows the variation of density of Al-1.8 Fe and Al-5 Fe composites with reaction temperature. The density is increased due to the porosity being decreased with Fe content and reaction temperature. This indicates that the densest bodies occur at 1200 °C, which can help improve the mechanical properties of composites.

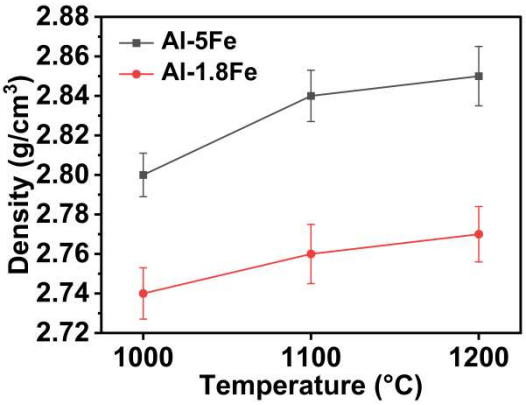

Fig. 4 Variation of density of Al-1.8Fe and Al-5Fe composites with reaction temperature.

3.4 Microstructure of composites

The Al-1.8 Fe alloy exhibits coarse Al grains and discontinuous Fe-rich phases along the grain boundaries (Fig. 5a), while the Al-5 Fe alloy shows the coarse Fe-rich phases (Fig. 5c), which severely segregate the Al matrix. In contrast, the microstructure of composites is significantly changed (Figs. 5c and 5d). In the Al-1.8 Fe composite, α-Al grains are refined and the Fe-rich phases are transformed into small particles, which reduce their detrimental fragmentation for Al matrix (Fig. 5b). In Al-5 Fe composite, the Fe-rich phases are transformed into finer and uniformly dispersed platelets (Fig. 5d).

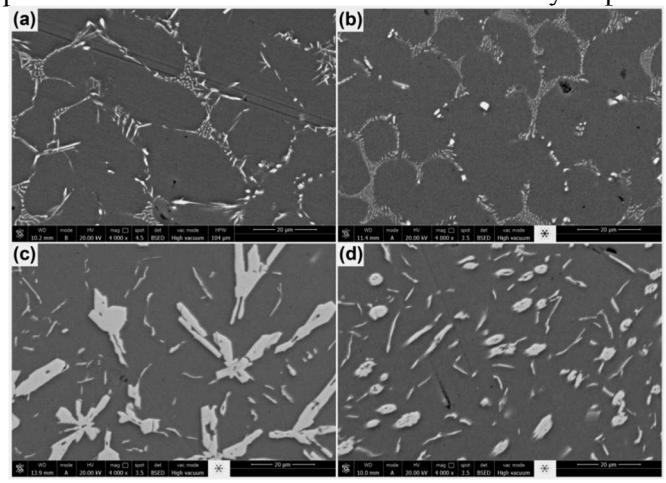

Fig. 5 SEM morphology of Al-Fe alloys and composites reacted at 1200 °C. (a) Al-1.8 Fe alloy，(b) Al-1.8Fe composite; (c) Al-5 Fe alloy; (d) Al-5 Fe composite.

Doi: https://doi.org/10.63333/eem.v2n11 Vol. 2 No. 1 (2026)

Fig. 6 shows the microstructure and EDS results of Al-1.8 Fe and Al-5 Fe composites. The atomic ratio of Al to O at Points A and C in Fig. 6a and b is approximately 2:3 as confirmed by the EDS spectra in Fig. 6a1 and a2, which corresponds to the stoichiometry of Al_2O_3, Points B and D contain Al and Fe with an atomic ratio of about 3:1, identified as the Al_3Fe phase (Fig. 6a1 and b2). The in-situ formed Al_2O_3 particles are mostly spherical with nano-submicron sizes (Fig. 6a and b). However, the TEM analysis did not observe the expected orientation relationship of the particles with Al matrix and Al_3Fe intermetallics. The refinement is regarded that the high-density and uniformly distributed Al_2O_3 particles effectively inhibit the growth of Al grains and intermetallics by pinning the phase boundaries in crystallization [23-25].

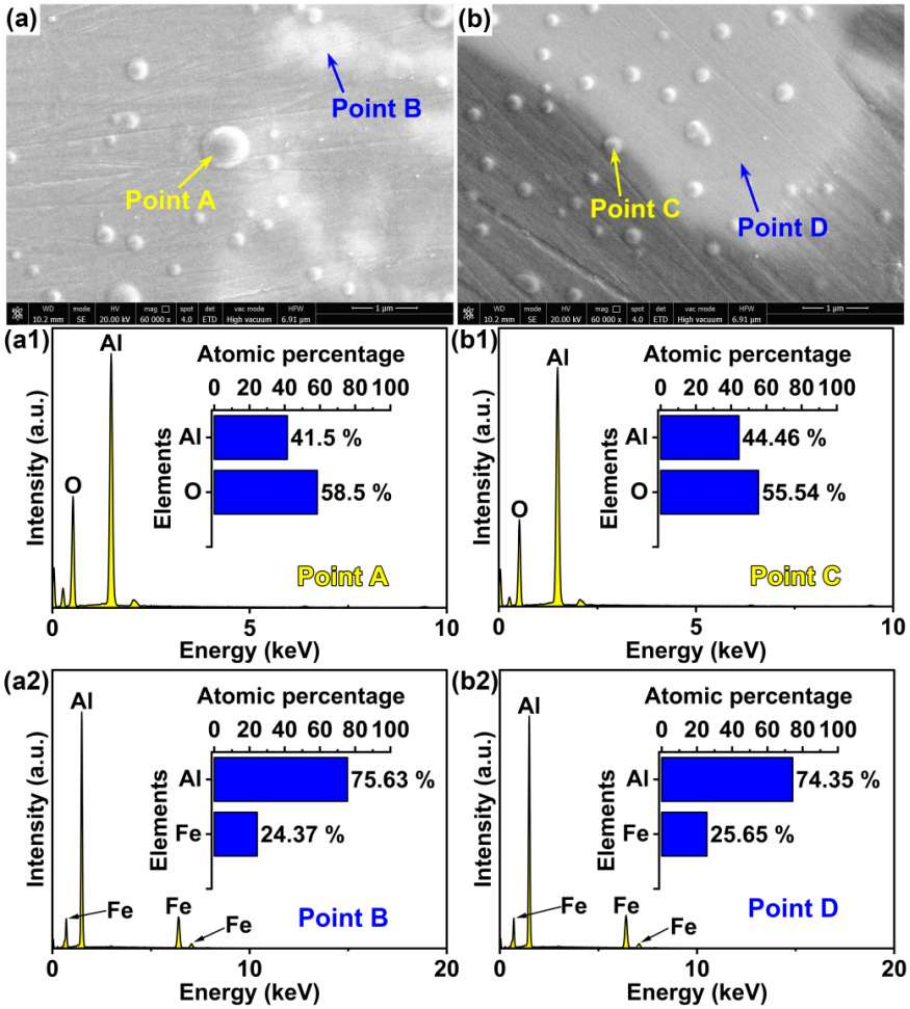

Fig. 6 Microstructure and EDS results of Al-Fe composites reacted at 1200 °C.
(a) Al-1.8 Fe composite; (a1 and a2) EDS result of Point A and B; (b) Al-5 Fe composite; (b1 and b2) EDS result of Point C and D.

3.5 Phase composition of composites

The phase composition of composites can also be identified by X-ray diffraction (Fig. 7). The peaks corresponding to Al and Al_3Fe were observed; no peak of Fe_2O_3 was identified. This indicates that the reaction between Al and Fe_2O_3 powder is completed in the stirring melts at 1200 °C for 30 min. The absence of diffraction peaks of Al_2O_3 is attributed to fact that these materials are composed of tens of microns, microns, submicrons, and nano grades of crystals; the diffraction peaks of the submicron and

Doi: https://doi.org/10.63333/eem.v2n11 Vol. 2 No. 1 (2026)

nanosized Al_2O_3 crystals are very weak compared to that of tens of micron crystals. They are submerged in the noise of background line, resulting in great difficulty in identifying the peaks.

To further disclose the characteristics of the Al_2O_3 particles, the composite samples were deeply etched in an HCl solution (20%) to completely remove Al matrix. By repeatedly washing, the remaining cleaned powder shows the morphology and phase composition (Fig. 8). They are exactly the spherical particles and have an α-Al_2O_3 structure. All of the characteristics confirm that the Al_2O_3 particle-reinforced Al-Fe composites are obtained through the in-situ reaction.

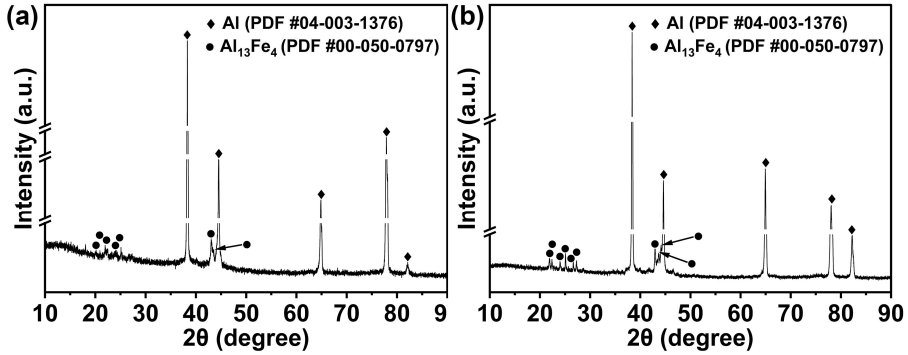

Fig. 7 XRD patterns of Al-Fe composites reacted at 1200 ℃
(a) Al-1.8 Fe; (b) Al-5 Fe.

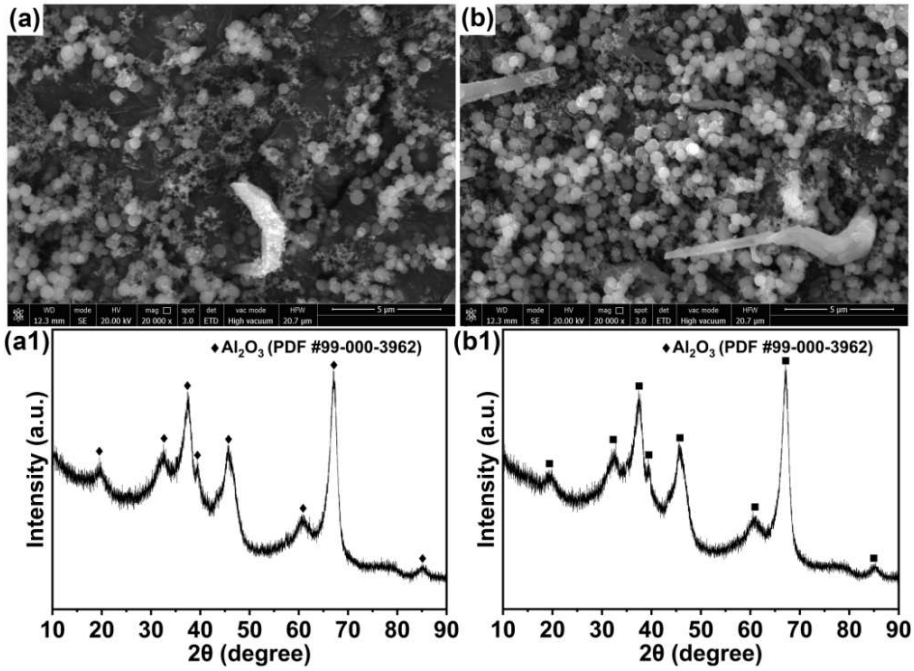

Fig. 8 SEM images and XRD patterns of the residual powder by removing Al matrix of composites. (a and a1) Al-1.8 Fe; (b and b1) Al-5 Fe.

3.6 Quantitative analysis of morphology and size of phases
3.6.1 Al_2O_3 particles

Doi: https://doi.org/10.63333/eem.v2n11 Vol. 2 No. 1 (2026)

The Al_2O_3 particles are embedded in the matrix and Al_3Fe phases (Fig. 9a and b). In the Al-1.8 Fe composite, the size of Al_2O_3 particles ranges from 0.05 to 0.4 μm, with an average size of 0.16 μm (Fig. 9a1). In Al-5 Fe composite, the size of Al_2O_3 particles ranges from 0.05 to 0.25 μm, with an average size of 0.14 μm (Fig. 9b2).

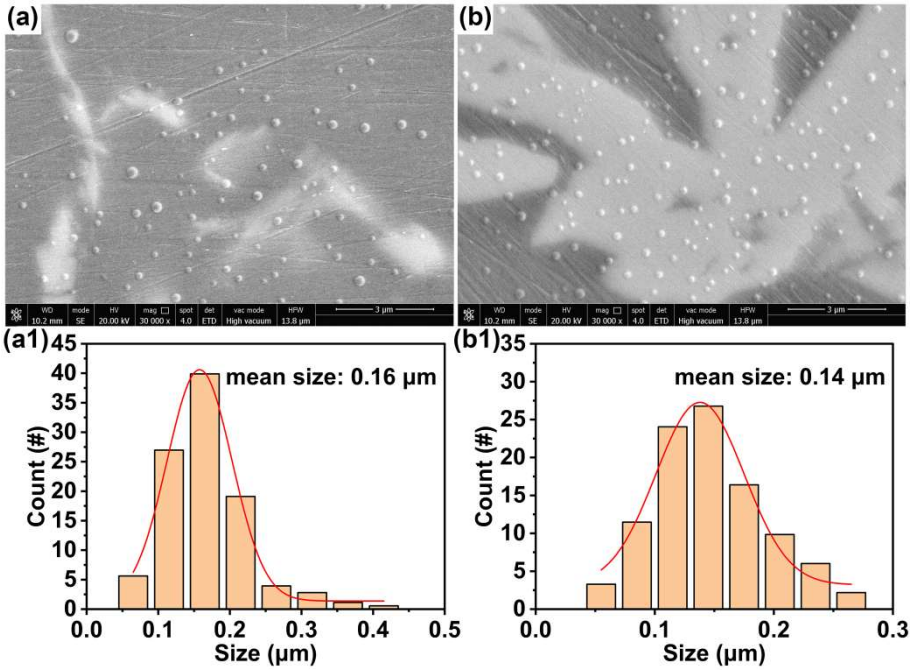

Fig. 9 Morphology and size distribution of Al_2O_3 particles. (a and a1) Al-1.8Fe composite; (b and b1) Al-5Fe composite.

3.6.2 Al grains

Introduction of Al_2O_3 particles leads to a significant refinement of Al grains in the composites (Figs. 10 and 11). The average Al grain size is reduced from 161.2 μm to 112.7 μm in Al-1.8Fe composite, corresponding to a refinement rate of 30.1%. Similarly, it is reduced from 152.1 μm to 99.2 μm in the Al-5 Fe composite, also achieving a refinement rate of 30.1%.

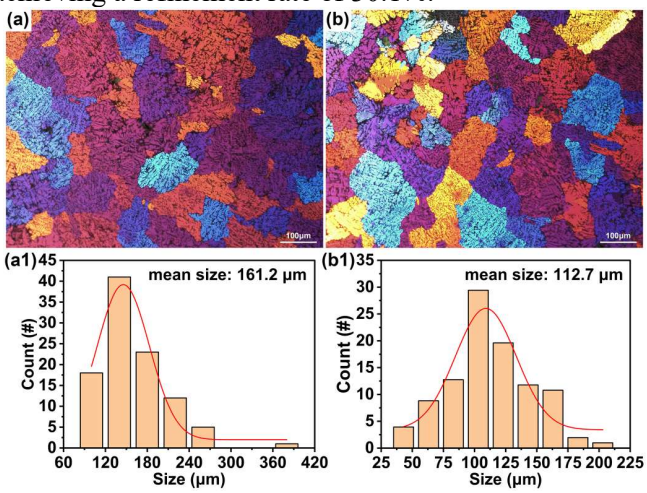

Fig. 10 Morphology and size distribution of Al grains. (a and a1) Al-1.8Fe Alloy; (b and b1) Al-1.8Fe composite.

Doi: https://doi.org/10.63333/eem.v2n11 Vol. 2 No. 1 (2026)

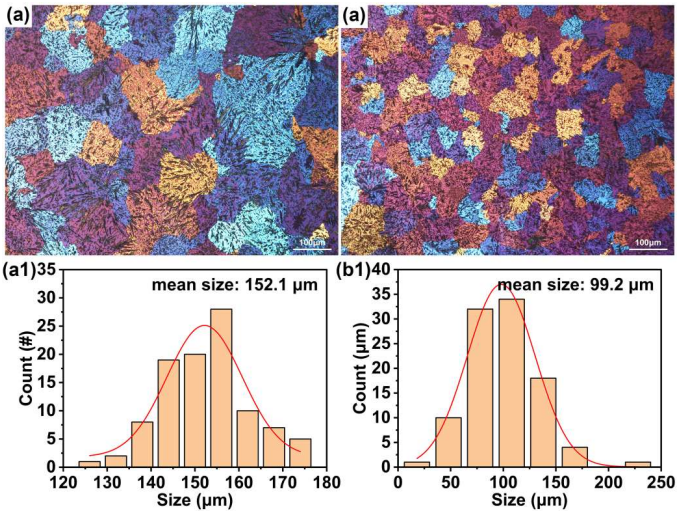

Fig. 11 Morphology and size distribution of Al grains. (a and a1) Al-5Fe Alloy; (b and b1) Al-5Fe composite.

The distribution characteristics of Al grains and Al_2O_3 particles in alloys and composites (Table 5) were statistically calculated on basis of Fig. 9, where d and d_0 represent the size of Al grains in alloys and composites respectively; λis the interparticle distance and f_v represents the volume fraction of Al_2O_3 particles. It was observed that the Al grains are refined by compositing and increasing Fe content, the size and interparticle distance of Al_2O_3 particles are reduced and the volume fraction is increased with increasing Fe content.

Table 5 The parameters of Al grains and Al_2O_3 particles in composites for calculations.

Samples	Al grains	Al_2O_3 particles			
	d	d_0	d	f_v	λ
Al-1.8 Fe	161.2 μm	112.7 μm	0.16 μm	1.27 vol %	1.1 μm
Al-5 Fe	152.1 μm	99.2 μm	0.14 μm	3.28 vol %	0.6 μm

3.7 Mechanical properties of composites

The yield strength, tensile strength, and elongation of Al-1.8 Fe alloy are low as 52.2 MPa, 100.7 MPa, and 3.0%, respectively. The corresponding properties of Al-1.8 Fe composite are increased to 77.2 MPa, 164.6 MPa, and 7.0%, improved by 32.3%, 52.7%, and 57.1%, respectively. The yield strength, tensile strength, and elongation of Al-5 Fe alloy are 64.1 MPa, 74.85 MPa, and 2.0%, respectively, while the properties of its composite are raised to 78.2 MPa, 153.2 MPa, and 5.0%, increasing by 18.0%, 51.1%, and 150% (Fig. 11).

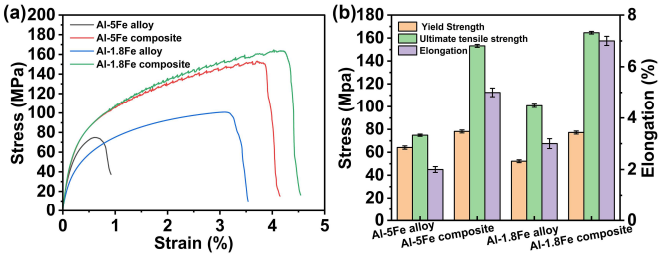

Fig. 12 Comparison of mechanical properties of alloys and the composites reacted at 1200 ℃. (a) Stress-strain curves; (b) YS, UTS, and EL.

Doi: https://doi.org/10.63333/eem.v2n11 Vol. 2 No. 1 (2026)

The hardness values of Al-1.8 Fe alloy and its composite are 84 HV and 118 HV, respectively (Fig. 12a), while those of Al-5Fe alloy and its composite are 180 HV and 228 HV, respectively (Fig. 12b). The hardness of composites is increased by 28.8% and 21.1%.

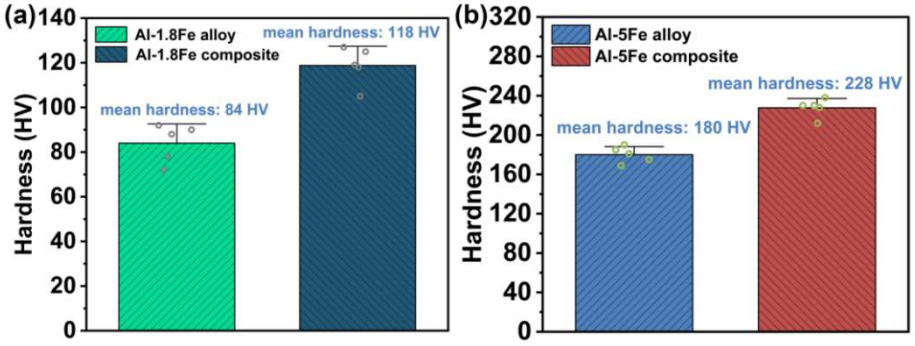

Fig. 13 Comparison of hardness of alloys and the composites.
(a) Al-1.8Fe alloy and Al-1.8Fe composite; (b) Al-5Fe alloy and Al-5Fe composite.

The improvements of mechanical properties greatly depend on the change in microstructure, in which the size of α-Al grains and the species, size, morphology, content, and distribution of the reinforcement phase are main factors to influence the mechanical properties of Al-Fe alloys. In the present, introduction of in-situ-produced fine Al_2O_3 particles largely improves the strength, plasticity, and hardness (Figs. 11 and 12); this is mainly ascribed to following factors. (1) The Al_2O_3 particles at boundaries enhance the interfacial resistance to cracking along the interfaces under loading [26]. (2) The densely and dispersively distributed Al_2O_3 particles largely strengthen the soft Al matrix and inhibit the movement of dislocations [27]. (3) The refined Al grains make dislocations migrate in more slipping directions, which has a positive effect on plastic deformation [28]. (4) The refined brittle Al_3Fe phases significantly reduce their segregation effect on the Al matrix and the stress concentration to delay cracking of the interfaces; the fine Al_3Fe particles play a similar resistant role in dislocation movement as Al_2O_3 particles do [29, 30].

The strengthening effect of Al grain refinement and dislocation (Orowan) on yield strength of materials induced by Al_2O_3 particles can be calculated using the following equations (4–6). The grain refinement-induced strengthening effect ($\Delta\sigma_{HP}$) was calculated using Hall-Petch relation [31, 32]:

$$\Delta\sigma_{HP}=k_y(d^{-1/2}-d_0^{-1/2}) \quad (4)$$

where, d and d_0 represent the grain sizes of Al in alloys and composites respectively (Fig. 7). k_y denotes the Hall-Petch coefficient for Al-Fe alloy [33]. The Orowan strengthening effect ($\Delta\sigma_{Orowan}$) can be calculated using following equations [34].

$$\Delta\sigma_{Orowan}=\frac{0.8Gb}{\lambda}\ln\frac{d}{2b} \quad (5)$$

$$\lambda=d\left[\left(\frac{1}{2f_v}\right)^{1/3}-1\right] \quad (6)$$

where, G is the shear modulus of the Al matrix, b is the Burgers vector of Al [35]. λ is the interparticle distance; d and f_v represent the average size and volume fraction of Al_2O_3 particles, which can be estimated from the distribution and size of Al_2O_3 particles (Fig. 9). The values of the parameters were given in Table 5.

The calculated values of $\Delta\sigma_{HP}$and $\Delta\sigma_{Orowan}$ are 6.5 MPa and 18.6 MPa for Al-1.8 Fe composite; the resulted total contribution (25.1 MPa) is in good agreement with the increment of experimental value (25 MPa). The calculated values of $\Delta\sigma_{HP}$and $\Delta\sigma_{Orowan}$ are 7.1 MPa and 32.8 MPa for Al-5Fe composite; the resulted total contribution (39.9 MPa) is nearly three times of the increment of experimental value, deviated seriously from the experimental results.

Doi: https://doi.org/10.63333/eem.v2n11 Vol. 2 No. 1 (2026)

The strengthening effect of Al_3Fe refinement can not be calculated because the Orowan mechanism is not suitable for large particles more than 1 μm [36]. Actually, the Al_3Fe phases in Al-5Fe composite still have negative influence on strength because they are not greatly refined; this must be the reason of the much higher calculation value than the experimental value.

Fig. 14 summarizes the mechanical properties of the Al-Fe alloys in this study and reported in literatures, highlighting the superiority of Al_2O_3 particle-reinforced Al-Fe composites. In conventional Al-Fe alloys, the mechanical performance is typically improved through the addition of alloying elements. However, when the added amount is limited, the resulting strength remains unsatisfactory. Conversely, an excessive addition tends to severe damage to the ductility of alloys. This indicates that the present Al_2O_3 particle-reinforced Al-Fe composites have outstanding advantages on mechanical properties when comparing to the alloys.

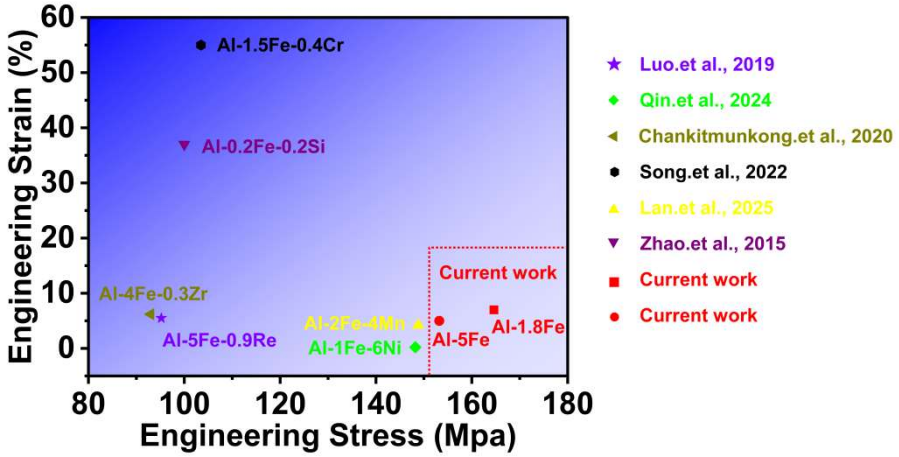

Fig. 14 Comparison of stress and strain between the present Al-Fe composite and other Al-Fe alloys [1, 6, 30, 37-39].

4. Conclusions

The Al_2O_3 particle-reinforced Al-Fe composite materials were fabricated through the in-situ reduction reaction of Fe_2O_3 powder in high-temperature Al melts.

The optimized preparation parameters are a melt temperature of 1200 °C, a reaction time of 30 min in stirring, and a preheat temperature of 200 °C for Fe_2O_3 powder.

The composites are composed of α-Al, Al_3Fe, and Al_2O_3 phases. The Al_2O_3 particles have a nano-submicron size and are densely dispersed in the matrix.

The fine Al_2O_3 particles play a crucial role in the refinement of both α-Al grains and Fe-rich phases by resisting their growth during solidification.

With an increase in amount of Fe_2O_3 powders, the number of Al_2O_3 particles is increased, leading to a more homogeneous distribution and significant refinement of α-Al grains and Fe-rich phases.

The yield strength, ultimate tensile strength, elongation, and hardness of composites are all improved through the in-situ reaction, which is enhanced with increasing the addition of Fe_2O_3 powders.

These composites have greatly refined microstructure and higher strength, plasticity, and hardness than the alloys, which are more suitable for preparation of assemblies used in energy and environment fields.

Acknowledgments

This work was supported by the Science and Technology Project of Inner Mongolia, China (Grant No. 2024KJHZ00₁7)

Conflict of Interest

The authors declare that there is no conflict of interest regarding the publication of this article.

Doi: https://doi.org/10.63333/eem.v2n11 Vol. 2 No. 1 (2026)

References

[1] Luo, S.X, Shi, Z.M, Li, N.Y, Lin, Y.M, Liang, Y.H, Zeng, Y.D. (2019). Crystallization inhibition and microstructure refinement of Al-5Fe alloys by addition of rare earth elements, J. Alloy Comp. 789, 90–99. https://doi.org/10.1016/j.jallcom.2019.03.071.

[2] Liang, Y.H, Shi, Z.M, Li, G.W, Zhang, R.Y, Zhao, G. (2019), Effects of Er addition on the crystallization characteristic and microstructure of Al-2wt%Fe cast alloy, J. Alloy Comp. 781, 235–244. https://doi.org/10.1016/j.jallcom.2018.12.063.

[3] Liang, Y.H, Shi, Z.M, Li, G.W, Zhang, R.Y, Li, M. (2019). Effects of rare earth modification on microstructure refinement and mechanical properties of Al-2 wt%Fe alloys, Mater. Res. Express 6, 106504 https://doi.org/10.1088/2053-1591/ab3$_5$bd.

[4] Song, X.Y, Gao, M.Q, Yang, B.W, Guan, R.G. (2022) , Modification and refinement of Fe-containing phases, mechanical properties and strengthening mechanisms in Al–Fe alloys via Cr alloying and continuous rheo-extrusion, Mater. Sci. Eng, A85$_0$, 143557. https://doi.org/10.1016/j.msea.2022.143557.

[5] Vončina, M, Medved, J, Steinacher, M, Ozimič, K. (2025). The influence of La and Ce additions on the solidification of alloys From the Al–Fe system, J. Therm. Anal. Calorim. 150, 873–882. https://doi.org/10.1007/s10$_9$73-024-13009-7.

[6] Qin, L.M, Tang, P, Meng, S.X. (2024). Effect of Ni addition on the microstructure, conductivities and mechanical properties of as-cast Al-Fe alloys, J. Alloy Comp. 986, 174160. https://doi.org/10.1016/j.jallcom.2024.174160.

[7] Nayak, S.S, Chang, H.J, Kim,D.H, Pabi, S.K. (2011) , Formation of metastable phases and nanocomposite structures in rapidly solidified Al–Fe alloys, Mater. Sci. Eng., A52$_8$, 5967-5973. https://doi.org/10.1016/j.msea.2011.04.028.

[8] Medvedev, A.E, Zhukova, O.O, Kazykhanov, V.U, Shaikhulova, A.F, Enikeev, N.A. (2022). On the effect of ECAP and subsequent cold rolling on the microstructure and properties of electromagnetically cast Al–Fe alloys, Int. J. Lightweight Mater. Manuf. 5, 484-495. https://doi.org/10.1016/j.ijlmm.2022.06.001.

[9] Chen, J.Q, Liu, C, Guan, R.G, Wen, F, Zhou, Q.Y, Zhao, H.J. (2020). Improving the comprehensive mechanical property of the rheo-extruded Al–Fe alloy by severe rolling deformation, J Mater Res Technol. 9, 1768–1779. https://doi.org/10.1016/j.jmrt.2019.12.008.

[10] Rong, X.D, Zhao, D.D, He, C.N, Zhao, N.Q. (2024). Review: recent progress in aluminum matrix composites reinforced by in situ oxide ceramics, J. Mater. Sci. 59, 9657–9684. https://doi.org/10.1007/s10$_8$53-023-09120-z.

[11] Lian, H, Shi, Z.M, Yu, W.L, Wang, Y, Wang, W.B, Pang, N. (2026) . Improvement of microstructure and mechanical property of Al–2Fe alloy through an in-situ reaction of Fe_2O_3 powder in Al–Mg melts, J Mater Res Technol. 411, 630–1643. https://doi.org/10.1016/j.jmrt.2026.01.072.

[12] Su, H, Gao, W.L, Feng, Z.H, Lu, Z. (2012) , Processing, microstructure and tensile properties of nano-sized Al_2O_3 particle reinforced aluminum matrix composites, Mater. Design 36, 590–596. https://doi.org/10.1016/j.matdes.2011.11.064.

[13] Wang, H.M, Li, G.R, Zhao, Y.T, Chen, G. (2010). In situ fabrication and microstructure of Al_2O_3 particles reinforced aluminum matrix composites, Mater. Sci. Eng., A52$_7$, 2881-2885. https://doi.org/10.1016/j.msea.2010.01.022.

[14] Zhu, H.G, Ai, Y.L, Li, J.L, Min, J, Chu. (2011), In situ fabrication of a-Al_2O_3 and Ni_2Al_3 reinforced aluminum matrix composites in an Al–Ni_2O_3 system, Adv. Powder. Technol. 22, 629–633. https://doi.org/10.1016/j.apt.2010.09.016.

[15] Jia, L.J, Rong, X.D, Zhao, D.D, Zhang, X, He, C.N, Zhao, N.Q. (2021). Microstructural characteristic and mechanical properties of the in-situ $MgAl_2O_4$ reinforced Al matrix composite based on Al-Mg-ZnO system, J. Alloy Comp. 891, 161991. https://doi.org/10.1016/j.jallcom.2021.161991.

[16] Li, H, Zhang, C, Han, X.D, Jiao, L, Shen, W.M, Song, Z.Y, Wang, J.H, Nie, Z.H, Shcheretskyi, O.

Doi: https://doi.org/10.63333/eem.v2n11 Vol. 2 No. 1 (2026)

(2025). Study on microstructural evolution and strengthening-toughening mechanisms of aluminum matrix composites fabricated by hot rolling and friction stir processing, J. Mater. Sci. 60, 15064–15086. https://doi.org/10.1007/s10853-025-11369-5.

[17] Patel, S.K, Shi, L. (2025). Recent Advances in Ceramic-Reinforced Aluminum Metal Matrix Composites: A Review, Alloys 4, 18. https://doi.org/10.3390/alloys40300018.

[18] Kai, X.Z, Huang, S.M, Wu, L, Tao, R, Peng, Y.J, Mao, Z.M, Chen, F, Li, G.R, Chen, G, Zhao, Y.T. (2019). High strength and high creep resistant ZrB_2/Al nanocomposites fabricated by ultrasonic-chemical in-situ reaction. J. Mater. Sci. Technol. 35, 2107–2114. https://doi.org/10.1016/j.jmst.2019.04.020.

[19] Gao, T, Liu, L.Y, Li, M.Y, Sun, Y, Wu, Y.Y, Liu, X.F. (2023). Design of Al based composites reinforced with in–situ Al_2O_3, AlB_2 and $Al11_3Fe_4$ particles, Compos. Commun. 40, 101629. https://doi.org/10.1016/j.coco.2023.101629.

[20] Azimi-Roeen, G, Kashani-Bozorg, S.F, Nosko, M, Švec, P. (2017). Reactive mechanism and mechanical properties of in-situ hybrid nano-composites fabricated from an Al–Fe_2O_3 system by friction stir processing, Mater. Charact. 127, 279–287. https://doi.org/10.1016/j.matchar.2017.03.007.

[21] Zhao, P.F, Shi, Z.M, Wang, X.F, Li, Y.Z, Cao, Z.Y, Zhao, M.D, Liang, J.H. (2023). A Review of the Laser Cladding of Metal-Based Alloys, Ceramic-Reinforced Composites, Amorphous Alloys, and High-Entropy Alloys on Aluminum Alloys, Lubricants 11, 482. https://doi.org/10.3390/lubricants11110482.

[22]Ye, D.L, Hu, J.H, Handbook of Practical Inorganic Thermodynamic Data. 2nd ed. Metallurgical industry press, Beijing 2002.

[23] Guo, Z.F, Liu, J, Sun, C.N, Maleksaeedi, S, Bi, G, Tan, M.J, Wei, J. (2014). Effects of nano-Al_2O_3 particle addition on grain structure evolution and mechanical behaviour of friction-stir-processed Al, Mater. Sci. Eng., A 602, 143–149. https://doi.org/10.1016/j.msea.2014.02.022.

[24] Ramezani, A, Jamshidi Avdal, H, Jamaati, R. (2025). Influence of Al_2O_3 addition on microstructure, mechanical strength, and wear behavior of AA7075-Al_2O_3 matrix composites fabricated using deformation-driven metallurgy, Rineng. 26, 104714. https://doi.org/10.1016/j.rineng.2025.104714.

[25] Xu, T, Li, G.R, Xie, M.L, Liu, M, Zhang, D, Zhao, Y.T, Chen, G, Kai, X.Z. (2019) Microstructure and mechanical properties of in-situ nano γ-Al_2O_3p/A356 aluminum matrix composite, J. Alloy Comp. 787, 72–85. https://doi.org/10.1016/j.jallcom.2019.02.045.

[26] Gyarmati, G, Erdélyi, J. (2025). Intermetallic phase control in cast aluminum alloys by utilizing heterogeneous nucleation on oxides, Metals 15, 404. https://doi.org/10.3390/met15040404.

[27] Qian, D.H, Wang, Y.F, Yao, Z.H, Chen, J, Yi, H, Chi, Y.M. (2025). Research Progress on Interfacial Bonding and Strengthening of Aluminum Matrix Composites, Int. J. Pr. Eng. Man-Gt. 6, 2288–6206 https://doi.org/10.1007/s40684-025-00798-x.

[28] Li, X.N, Liu, Z.Y, Luo,H.J, Ma, K, Xiao, B.L, Wang, D, Ma, Z.Y. (2023). Enhancing strength-ductility synergy of graphene/Al-Cu-Mg composites via forming $MgAl_2O_4$@graphene complex structure, Compos. Commun. 43, 101737. https://doi.org/10.1016/j.coco.2023.101737.

[29] Zhang, Z, Nie, K.B, Deng, K.K, Xu, C. (2024). Preparation of low-cost, high-strength and fast-dissolving (MgO-Al_3Fe)/AZ91 magnesium matrix composites using a novel in-situ reaction, Compos. Commun. 49, 101986. https://doi.org/10.1016/j.coco.2024.101986.

[30] Chankitmunkong, S, Eskin, D.G, Limmaneevichitr, C. (2020). Structure refinement, mechanical properties and feasibility of deformation of hypereutectic Al-Fe-Zr and Al-Ni-Zr alloys subjected to ultrasonic melt processing, Mater Sci Eng, A788, 139567. https://doi.org/10.1016/j.msea.2020.139567.

[31] Pu, B.W, Lin, X.B, Li, B.W, Chen, X.F, He, C.N, Zhao, N.Q. (2020). Effect of SiC nanoparticles on the precipitation behavior and mechanical properties of 7075Al alloy, J. Mater. Sci. 55, 6145–6160. https://doi.org/10.1007/s10853-020-04381-4.

[32] Chen, Y.Y, Nie, J.F, Wang, F, Yang, H.B, Wu, C.C, Liu, X.F, Zhao, Y.H. (2020). Revealing hetero-

Doi: https://doi.org/10.63333/eem.v2n11 Vol. 2 No. 1 (2026)

deformation induced (HDI) stress strengthening effect in laminated Al-(TiB_2+TiC)p/6063 composites prepared by accumulative roll bonding, J. Alloy Compd. 815, 152285. https://doi.org/10.1016/j.jallcom.2019.152285.

[33] Sharma, A, Morisada, Y, Ushioda, K, Fujii, H. (2024). Elucidation of the factors controlling interface decohesion and particle fracture in a friction stir alloyed Al–Fe alloy system, Materialia 34, 102066. https://doi.org/10.1016/j.mtla.2024.102066.

[34] Zhang, Q, Xiao, B.L, Wang, W.G, Ma, Z.Y. (2012). Reactive mechanism and mechanical properties of in situ composites fabricated from an Al-TiO_2 system by friction stir processing. Acta Mater. 60, 7090–7103. https://doi.org/10.1016/j.actamat.2012.09.016.

[35] Fribourg, G, Brechet, Y, Deschamps, A, Simar, A. (2011). Microstructure-based modelling of isotropic and kinematic strain hardening in a precipitation-hardened aluminium alloy, Acta Mater. 59, 3621–3635. https://doi.org/10.1016/j.actamat.2011.02.035.

[36] Xu, Z.H, Zhang, X, Zhao, N.Q, He, C.N. (2020). Synergistic strengthening effect of in-situ synthesized WC_1-x nanoparticles and graphene nanosheets in copper matrix composites, Compos. Appl. Sci. Manuf. 133 , 105891. https://doi.org/10.1016/j.compositesa.2020.105891.

[37] Song, X.Y, Gao, M.Q, Yang, B.W, Guan, R.G. (2022). Modification and refinement of Fe-containing phases, mechanical properties and strengthening mechanisms in Al–Fe alloys via Cr alloying and continuous rheo-extrusion, Mater Sci Eng, A 850, 143557. https://doi.org/10.1016/j.msea.2022.143557.

[38] Lan, X.Y, Zhang, Y.P, Li, K, Hu, B, Wang, J, Lu, Q, Wen, J.Y, Zhang, X, Du,Y. (2025). Investigation into the correlation between composition, microstructure, and mechanical properties of Al-xFe-(6-x)Mn alloys, J. Alloy Compd. 1036, 181455. https://doi.org/10.1016/j.jallcom.2025.181455.

[39] Zhao, Q.R, Qian, Z, Cui, X.L, Wu, Y.Y, Lu, X.F. (2015). Optimizing microstructures of dilute Al-Fe-Si alloys designed with enhanced electrical conductivity and tensile strength, J. Alloy Compd. 650, 768–776. http://dx.doi.org/10.1016/j.jallcom.2015.08.052.